Crystallization Process of Amorphous Fe-Ta-C Alloy Films and Thermal Stability of the Resultant Soft-Magnetic Nanocrystalline State

Materials Transactions, JIM, Vol. 36, No. 7 (1995), pp. 952 to 961

Crystallization Process of Amorphous Fe-Ta-C Alloy Films and Thermal Stability of the Resultant Soft-Magnetic Nanocrystalline State†

N. Hasegawa*, A. Makino*, N. Kataoka**††,
H. Fujimori**, A. P. Tsai**, A. Inoue**
and T. Masumoto**

*Nagaoka Branch, Central Research Laboratory, Alps Electric Co., Ltd., Nagaoka 940, Japan
**Institute for Materials Research, Tohoku University, Sendai 980-77, Japan

Nanocrystallization behavior in sputter-deposited amorphous Fe-Ta-C films has been studied. By an analysis of kinetics combined with the microstructural characterization, it was found that the first stage reaction is primary crystallization of α-Fe, which is similar to that occurs in amorphous Fe-Cu-Nb-Si-B and Fe-M-B (M=Zr, Hf, or Nb) alloys. The precipitation of TaC crystals follows this reaction, though some bonding between Ta and C seems to be already present in the amorphous matrix. In the early stage, the growth of primary α-Fe grain is considered to be suppressed by the solute-enriched amorphous matrix, being similar to the other nanocrystalline alloys mentioned above. However, such a partially crystallized state is not an optimum state for soft magnetic properties unlike the others, because the residual amorphous phase has only a low magnetization resulting in an insufficient intergranular magnetic coupling. After an optimum annealing of the film with the optimum composition, the residual amorphous phase is almost absent and the TaC particles dispersed at grain boundaries of α-Fe play an important role for retarding the grain growth instead. The temperature range where the residual amorphous phase exists is considerably narrow compared with the other nanocrystalline alloys, probably because the reactivity between Ta and C toward TaC is stronger than that between M and B, and hence the residual amorphous phase easily decomposes. The relation between structural evolution after nanocrystallization and magnetic softness was also investigated for the films outside the optimum composition.

(Received January 6, 1995)

Keywords: *amorphous alloy, nanocrystalline, iron base alloy, soft magnetic property, sputter deposition, thin film, crystallization kinetics, thermal stability, dispersed carbide particle, transmission electron microscopy*

I. Introduction

Recently, nanocrystalline metallic materials produced by crystallization of amorphous alloys attract much attention from a viewpoint of industrial applications, because of their promising characteristics as high magnetization soft magnets (Fe-Cu-Nb-Si-B[1], Fe-M-B (M=Zr, Hf, or Nb)[2][3], etc.) or high strength materials (Al-Ni-X (X=Y, Ce, or Nd)[4][5], etc.). The generation of a large number of nuclei at an early annealing stage is needed for nanocrystallization from amorphous phase. For the Fe-Cu-Nb-Si-B alloys, compositional inhomogeneity evolves in the amorphous phase owing to the immiscibility of Cu in Fe, resulting in the increased number density of the heterogeneous nucleation sites[6]. The reaction at the first stage of crystallization of those alloys is explained as primary crystallization[7]-[9], which accompanies long range diffusion and partitioning of solute elements. This reaction results in a composite microstructure composed of the primary α nanocrystals and the M- or X-enriched residual amorphous phase. For this type of alloys, grain growth of nanocrystals is considerably retarded owing to the small diffusivity of M or X which is rejected from the crystallized region and enriched in the residual amorphous phase.

Nanocrystalline Fe-Ta-C alloy films are also known as high magnetization soft magnetic materials produced by crystallization of sputter-deposited amorphous films[10]. In these films, the generation of copious nuclei in an amorphous phase is believed to be associated with the development of nanoscaled concentration fluctuations of C[11]. After an optimum annealing of the film with an optimum composition, the film is composed of α-Fe and small tantalum-carbide particles (TaC with the NaCl type cubic crystal structure) which is located at the grain boundaries of α-Fe[12]. However, the precipitation mechanism of the α-Fe and TaC, in particular, the question which phase precipitates first, has not been fully understood yet. If the crystallization process is similar to that of the Fe-Cu-Nb-Si-B or the Fe-M-B alloys, the primary α-Fe phase would precipitate from the amorphous matrix first. Previous high-resolution TEM observations[12] failed to confirm the presence of the residual amorphous phase in the optimum stage, unlike in the case of the Fe-Cu-Nb-Si-B and the Fe-M-B alloys. The

† A part of this paper was presented at the 1991 Autumn Meeting of Japan Institute of Metals.
†† Passed away on June 27, 1994.

aim of this paper is to clarify the difference and/or similarity in the crystallization process between Fe-Ta-C alloys and other amorphous alloys which form nanocrystalline microstructures by primary crystallization.

II. Experimental Procedure

Amorphous Fe-Ta-C alloy films with 5 μm in thickness were prepared by rf sputtering. The detailed deposition conditions are described elsewhere[13]. Isothermal crystallization kinetics was analyzed by two different methods. One is differential scanning calorimetry (DSC) and the other is saturation magnetization measurement by vibrating sample magnetometer (VSM) during isothermal crystallization. Crystallization kinetics at a constant heating rate was also measured by differential thermal analysis (DTA) and VSM. Microstructures were investigated by transmission electron microcopy (TEM). A field-emission-type 200 kV TEM (JEOL JEM-2010F) was used for high-resolution observations combined with nanobeam EDX (energy dispersive X-ray spectroscopy) analyses, for which a probe diameter of 0.5 nm was employed. A conventional 200 kV TEM (JEOL JEM-2000EX) was used for bright-field and dark-field observations. The Fe-Ta-C films were peeled off from the substrates and then ion-milled from both sides to prepare thin specimens for TEM observations. ^{57}Fe Mössbauer effect measurements were made for identification of the secondary magnetic phase (other than α-Fe) that could not be detected by electron diffractometry of crystallized samples. Mössbauer spectra were measured at room temperature by a conventional constant-acceleration-type spectrometer using a ^{57}Co source doped with Rh. Coercivity at room temperature and the temperature dependence of coercivity were measured by a dc *B-H* loop tracer and VSM, respectively.

III. Results and Discussion

1. Microstructural observations and crystallization kinetics

(1) Microstructure at an early stage of crystallization

A typical film with the alloy composition of $Fe_{81.4}Ta_{8.3}C_{10.3}$ (at%), which shows good soft magnetic properties after annealing around 750-1000 K, was chosen as a sample for the present analyses of crystallization behavior. The structure of the as-deposited film of this composition is amorphous. Figure 1 shows the bright-field and dark-field TEM images and electron diffraction patterns of the film after isochronal annealing (for 1.2 ks) at various temperatures. In the film annealed at 718 K for 1.2 ks (Fig. 1(c)), the crystallization seems to be almost completed, and it consists of α-Fe(bcc) and TaC nanocrystals as identified by the electron diffraction pattern. After annealing at lower temperatures, however, diffraction rings from TaC are not recognized and only bcc nanocrystals are visible, embedded in the amorphous matrix (Fig. 1(a) and (b)).

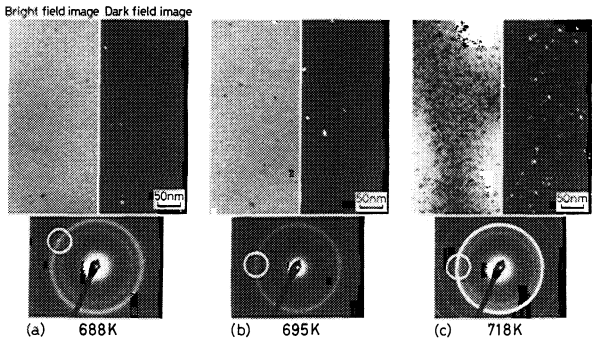

Fig. 1 TEM images and electron diffraction patterns of the $Fe_{81.4}Ta_{8.3}C_{10.3}$ alloy films annealed for 1.2 ks at various temperatures. The dark-field images were taken with an objective aperture indicated with the circles in the diffraction patterns.

To clarify the microstructure of these partially crystallized films further, high-resolution FE-TEM observation combined with nanobeam EDX analysis was performed for the film annealed at 688 K. The result is shown in Fig. 2. As seen in the EDX spectra, Ta concentration of the bcc nanograin is less than that of the amorphous matrix. This means that the transformation in this alloy is not a polymorphic crystallization but a primary crystallization accompanying relatively long range diffusion of Ta (and C) atoms. Since α-Fe has only a few atomic percent of solubility with Ta, Ta atoms must be rejected from the crystallized region. However, the present EDX analysis suggests the considerable supersaturation of Ta in α-Fe, as already suggested by the atom probe FIM analysis of a fully crystallized sample[11]. (The atom probe analysis also suggested the supersaturation of C.) The excessively dissolved Ta (and C) in α-Fe is gradually rejected by higher-temperature or longer annealing, as evidenced by X-ray diffractometry which shows that the expanded lattice spacing of α-Fe decreases and approaches that of pure-Fe[13].

Another concern about the partially crystallized sample is whether TaC crystals are present inside the residual amorphous phase or not. If the TaC crystal is present, it can easily be distinguished from the α-Fe crystals in the high-resolution TEM image, because the widest lattice spacing of TaC (0.257 nm for {111}) is sufficiently larger than {110} plane distance of α-Fe (0.203 nm). As seen in Fig. 2, clearly ordered region (larger than 2 nm in diam.) with the lattice friges larger than those of {110} of α-Fe is hardly seen in the residual amorphous phase. However, some medium-range order can be seen in the amorphous matrix in Fig. 2 and there is a secondary halo, which reflects the presence of atomic distance close to the {111} or {200} plane distance of TaC, inside the main halo ring in the diffraction pattern of Fig. 1(a). Though TaC crystals are not present at this stage, there may be some bonding between Ta and C in amorphous matrix. The factor that reduce the grain growth rate of α-Fe is a small diffusion coefficient of Ta. Since a large grain cannot easily relieve the lattice strain caused by supersaturation of Ta, grain growth would naturally be controlled by the slug-

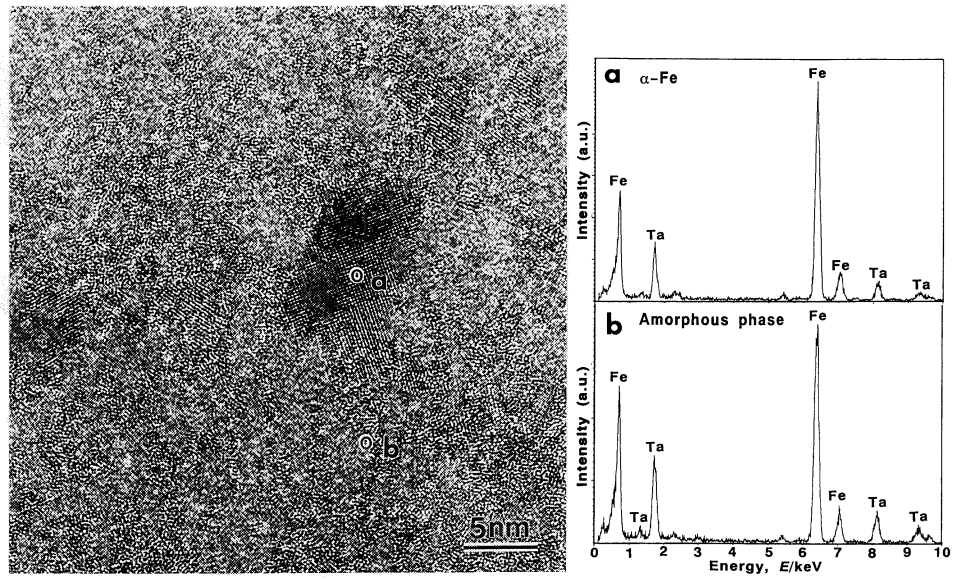

Fig. 2 High-resolution TEM image and nanobeam EDX spectra of the $Fe_{81.4}Ta_{8.3}C_{10.3}$ alloy film annealed at 688 K for 1.2 ks. The EDX spectra a and b were taken from the points indicated with the circles in the photograph.

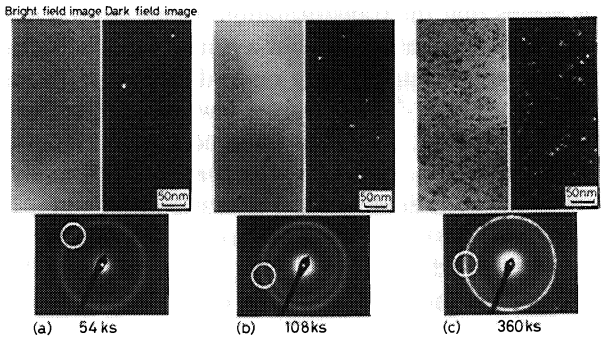

Fig. 3 TEM images and electron diffraction patterns of the $Fe_{81.4}Ta_{8.3}C_{10.3}$ alloy films showing the isothermal structural change at 658 K. The dark-field images were taken with an objective aperture indicated with the circles in the diffraction patterns.

gish diffusion of Ta out of α-Fe. The rejected Ta from α-Fe would be especially enriched near the boundaries of α-Fe grains and again serves to suppress the growth.

Figure 3 shows a series of TEM images and electron diffraction patterns showing structural changes by isothermal annealing at 658 K. (The film composition is the same as above.) After annealing for 360 ks, crystallization seems to be almost completed. The structure of this film aged for a longer time at relatively low temperature is basically the same as shown in Fig. 1(c) which was annealed for a shorter time at relatively high temperature. At an early stage, primary α-Fe nanocrystals precipitate in the amorphous matrix and the number of the α-Fe grain increases as annealing time, as can be seen in Fig. 3(a)–(c). On the other hand, the grain growth rate is extremely slow and the noticeable difference in the grain size is not observed in Fig. 3(a)–(c). This is reasonable considering that the grain growth rate generally decreases as aging proceeds, typically following a parabolic law, for diffusion controlled growth.

(2) Kinetics of crystallization

Figure 4 shows the isothermal DSC curves for nanocrystallization of the $Fe_{81.4}Ta_{8.3}C_{10.3}$ alloy film. There is an incubation period t_i before exothermic reaction takes place. The fraction transformed X was calculated by integrating these DSC curves. In Fig. 5, $-\ln(1-X)$ was plotted logarithmically against logarithm of time t $(=t_a-t_i)$ from the onset of the crystallization. (t_a is the annealing time during DSC measurement.) As can be seen in the figure, these plots fall into straight lines within a X range of 0.2–0.7. This means that the crystallization of the present alloy proceeds by the nucleation-and-growth process following the Johnson-Mehl-Avrami (JMA) equation[14][15] given by

$$X=1-\exp(-kt^n), \tag{1}$$

where n is known as the Avrami exponent which depends

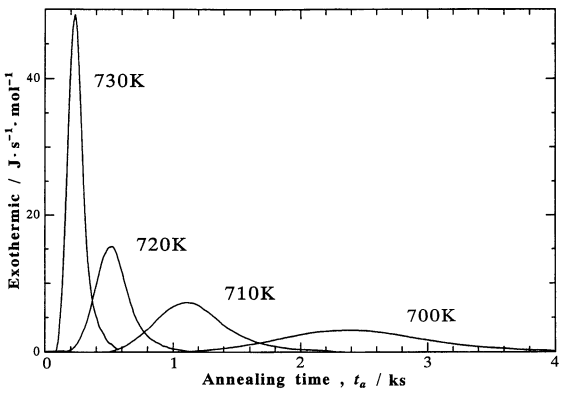

Fig. 4 Isothermal DSC curves for nanocrystallization of the $Fe_{81.4}Ta_{8.3}C_{10.3}$ alloy films.

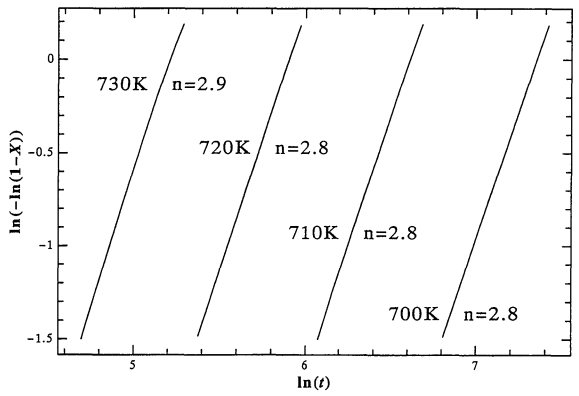

Fig. 5 Johnson-Mehl-Avrami plot of the isothermal DSC results for nanocrystallization of the $Fe_{81.4}Ta_{8.3}C_{10.3}$ alloy films.

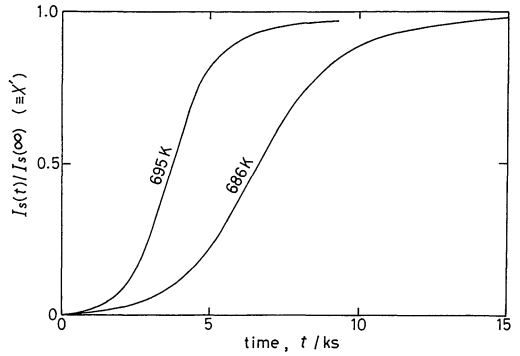

Fig. 6 Isothermal variation of the reduced saturation magnetization of the $Fe_{81.4}Ta_{8.3}C_{10.3}$ alloy films.

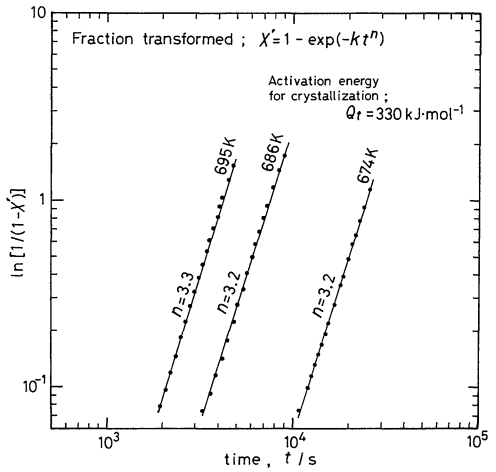

Fig. 7 Johnson-Mehl-Avrami plot of the results of isothermal magnetization measurment for the $Fe_{81.4}Ta_{8.3}C_{10.3}$ alloy films.

on the nucleation mechanism and growth morphology and k is a kinetic (rate) parameter. In contrast with the Fe-M-B alloys whose n decreases with decreasing temperature[9] and the Fe-Cu-Nb-Si-B alloys whose n changes into a smaller value when X exceeds 0.5[16], the n(=2.8-2.9) of the present alloy film is almost independent of temperature and X. This means that the nucleation mechanism and growth morphology of the present alloy are almost constant irrespective of temperature and time. The apparent activation energy for crystallization estimated by an Arrhenius plot of the annealing time needed to reach the exothermic peak from the start of transformation is 340 kJ/mol (3.5 eV), which is a common value for ordinary metal-metalloid amorphous alloys.

Since both the α-Fe and TaC crystals are present after the exothermic reaction, the exothermic curve must be the result of an overall reactions containing precipitation of α-Fe and TaC (though eutectoid reaction is unlikely as described later). In order to analyze the crystallization kinetics of α-Fe separately, time dependence of saturation magnetization was measured. Since the Curie temperature of the amorphous phase is well below the temperature at which the crystallization occurs (as seen in Fig. 12), magnetization measured at the annealing temperatures is believed to be directly proportional to the volume fraction transformed into α-Fe. The increase in saturation magnetization of α-Fe itself due to the rejection of supersaturated Ta and C is believed to be negligible, because the lattice spacing of α-Fe decreases only by about 0.1% in the course of this transformation. Figure 6 shows the time dependence of the fraction transformed for α-Fe (denoted as X') that is the saturation magnetization $Is(t)$ normalized by the Is of fully crystallized sample. The time taken as abscissa of Fig. 6 does not include incubation periods. These curves show sigmoidal shape which is typical of the nucleation-and-growth process. Figure 7 shows the JMA plots of X' for three different temperatures. These plots again yield straight lines within a X' range of 0.1-0.8. By an Arrhenius plot of t needed to reach X' of 0.5, the apparent activation energy for crystallization of α-Fe was estimated to be 330 kJ/mol (3.4 eV), which is almost identical with that estimated by the DSC measurement. Besides, the Avrami exponent n given by the magnetization measurement (3.2-3.3) was close to that given by the DSC measurement (2.8-2.9). Such agreement in the activation energy and n measured by the two different methods implies that the precipitated TaC crystals are so small that DSC could not detect their crystallization and yielded only a single exothermic peak. The possibility of an eutectoid reaction resulting in a simultaneous precipitation of α-Fe and TaC is excluded considering the microstructural evolution as shown in Fig. 3.

It is known that the Avrami exponent n is separated into two components[17]

$$n=a+bp \tag{2}$$

where a is the nucleation rate component which varies from $a=0$ for instantaneous nucleation to $a=1$ for a constant nucleation rate, b defines the dimensionality of growth, and $p=1$ for interface-controlled growth and 0.5 for diffusion-controlled growth. The quantity b for the present alloy is 3, because the shape of grain is three-dimensionaly isotropic. Assuming the diffusion-controlled growth ($p=0.5$), the measured n of 2.8-3.3 for the present alloy suggests the constant (or increasing)

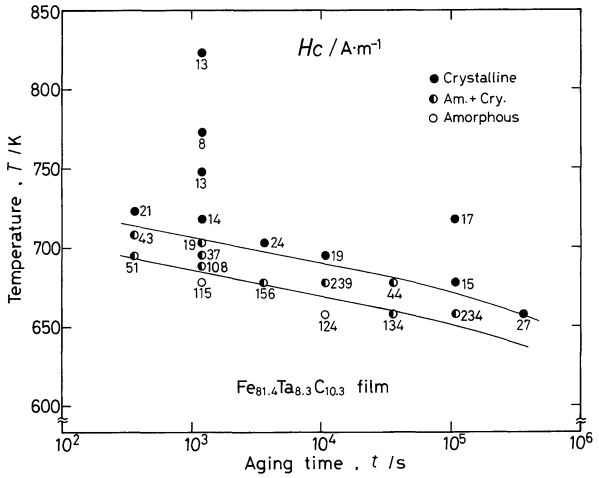

Fig. 8 Time-temperature-transformation diagram of the $Fe_{81.4}Ta_{8.3}C_{10.3}$ alloy film. Coercivity is also indicated.

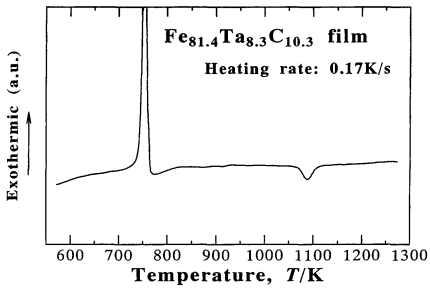

Fig. 9 DTA curve of amorphous $Fe_{81.4}Ta_{8.3}C_{10.3}$ alloy film measured at a constant heating rate.

nucleation rate. This is in contrast to the case of Fe-Cu-Nb-Si-B or Fe-M-B alloys for which the presence of pre-existing nucleation center is suggested[16][9] because of the smaller n's (1.0-2.1).

Figure 8 shows the time-temperature-transformation (TTT) diagram together with the coercivity *Hc* for the Fe-Ta-C alloy of the same composition as above. As described before, the structure of the film after the completion of crystallization is nearly the same irrespective of temperature. This is again in contrast to the case of the Fe-M-B alloys for which the n and the resultant microstructure is dependent on annealing temperature[9]. The obtained low coercivity at every aging temperature for fully crystallized samples in Fig. 8 reflects the unchanged microstructure. This means that good soft magnetic properties can be reached without imposing any strict condition on the temperature and time of the heat treatment. In addition, it is also noted from Fig. 8 that the coercivity of the partially crystallized films is relatively high. This is probably caused by the weakness of ferromagnetic intergranular coupling, resulting in an insufficient decrement of effective magnetocrystalline anisotropy of α-Fe, due to the low magnetization of the residual amorphous phase present between α-Fe grains.

2. Thermal stability of nanocrystalline structure and soft magnetic properties

(1) Stabilization of nanograins in the optimum state

As described in the previous section, the precipitation process of α-Fe grains in the amorphous Fe-Ta-C films is the primary crystallization similar to those of the Fe-Cu-Nb-Si-B and the Fe-M-B alloys, although there is some possibility that the nucleation mechanism is different. Also, like the other alloys, the grain growth of the α-Fe nanograins at an early stage of crystallization is considered to be retarded by sluggish diffusion of Ta rather than by TaC crystals, because TaC has not been observed in the early stage. However, in the later stage, TaC precipitates pin the grain boundaries and retards the grain growth. It is of interest which is important for the stabilization of nanograins in an optimum condition for soft magnetic properties.

If an amorphous phase still remains after the first transformation, it will crystallize at higher-temperatures. Figure 9 shows the DTA curve of the $Fe_{81.4}Ta_{8.3}C_{10.3}$ alloy film measured at a constant heating rate of 0.17 K/s. The large exothermic peak seen around 750 K is due to the first stage crystallization discussed in the previous section. However, no clear exthothermic peaks are seen other than the principal peak. (The endothermic peak seen around 1070 K is due to the magnetic transformation of α-Fe, because the same endothermic peak appeared by rerunning the same DTA program for the same sample after heating up to 1273 K.) The absense of a secondary exthothermic peak in high-temperature region for this alloy is different from the Fe-Cu-Nb-Si-B[18] or the Fe-M-B[9] alloys.

If a ferromagnetic amorphous phase surrounds individual α-Fe grains, more sensitive way for detecting it is to measure the temperature dependence of coercivity *Hc*. Intergranular exchange coupling plays an important role in averaging out the magnetocrystalline anisotropy of α-Fe[19]. Since the exchange coupling is generally interrupted even by a insertion of a few atomic layer of the non-mag-

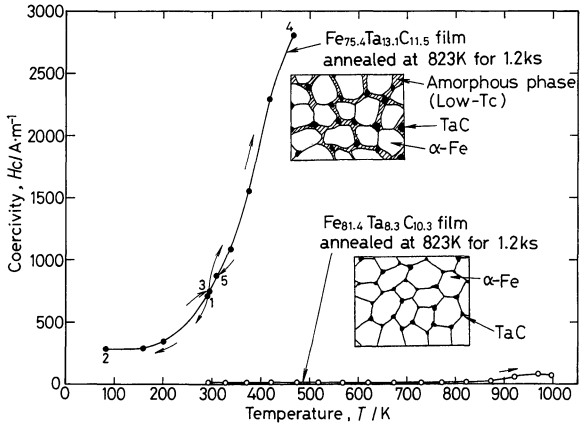

Fig. 10 Temperature dependence of coercivity *Hc* measured after pre-annealing at 823 K for 1.2 ks for $Fe_{81.4}Ta_{8.3}C_{10.3}$ film with near the optimum composition and $Fe_{75.4}Ta_{13.1}C_{11.5}$ film with excess Ta. Schematic views of microstructure for each film are also illustrated.

netic phase, the disappearance of magnetization of the amorphous phase surrounding α-Fe will bring about the increase of *Hc*. Figure 10 shows the temperature dependence of *Hc* for Fe–Ta–C alloy films of two different compositions. They were both pre-annealed at 823 K for 1.2 ks. As can be seen in the figure, the low *Hc* is maintained in the $Fe_{81.4}Ta_{8.3}C_{10.3}$ film (which is the optimum composition for the magnetic softness) below 823 K. The increase in *Hc* at higher temperature than 823 K is an irreversible change due to the gradual grain growth. On the contrary, the steep increase in *Hc* around 300 K was observed in $Fe_{75.4}Ta_{13.1}C_{11.5}$ film. This film has higher Ta concentration and higher Ta to C ratio than the optimum composition. As can be seen from the measurement sequence indicated by arrows and numerical labels in the figure, this change in *Hc* is reversible. This means that the exchange coupling is lost due to the existence of residual amorphous phase with low Curie temperature in the Ta-rich Fe–Ta–C film. Such a phase has not been detected in the film with nearly the optimum composition. Figure 11 shows the high-resolution TEM image together with the electron diffraction pattern and the EDX spectra for the Ta-rich alloy film annealed at 823 K. The diffraction pattern indicates the coexistence of α-Fe and TaC crystals. As mentioned above, TaC can easily be distinguished from α-Fe by its wider fringes. The grain size of α-Fe is 10–20 nm and the diameter of TaC is in the range of 3–7 nm. The nanobeam EDX spectra taken from the points indicated with the circles display the high intensity of Fe in the α-Fe grain (a) and the high intensity of Ta in the TaC grain (c), as expected. The EDX spectrum taken from the intergranular amorphous region (b) shows the intermediate composition. A schematic microstructure of this Ta-rich film is illustrated in Fig. 10 together with that of the film with the optimum composition (illustrated in the lower part).

The presence of such a residue of amorphous phase depending on the Ta concentration will be explained as follows. Both Ta and C atoms in the residual amorphous Fe–Ta–C phase will promptly be consumed by the precipitation and growth of TaC on annealing at sufficiently higher temperatures than that for the principal crystallization peak. If the C concentration in the film is equal to or higher than the Ta concentration, all the Ta atoms in the residual amorphous phase will be consumed to form TaC. In such a case, the residual amorphous phase can no longer be stable because crystallization temperature of Fe–C amorphous alloys is not so high. On the other hand, higher amount of Ta and C in the film will increase the crystallization temperature of the residual amorphous phase. Furthermore, for the films with the Ta concentration more than C concentration, the residue of Ta atoms after the formation of TaC can remain in the amorphous phase and serves to stabilize it. However, good soft magnetic properties can hardly be attained in such films because the magnetization of the residual amorphous phase expected at room temperature is considerably low.

Such a structural difference between the Ta-rich film and the optimum film is also reflected in the temperature dependence of saturation magnetization *Is*. Figure 12 shows the *Is*-*T* curves for the as-deposited films. The onset of primary crystallization at which the *Is* steeply increases for the Ta-rich film (a) is higher than that for the

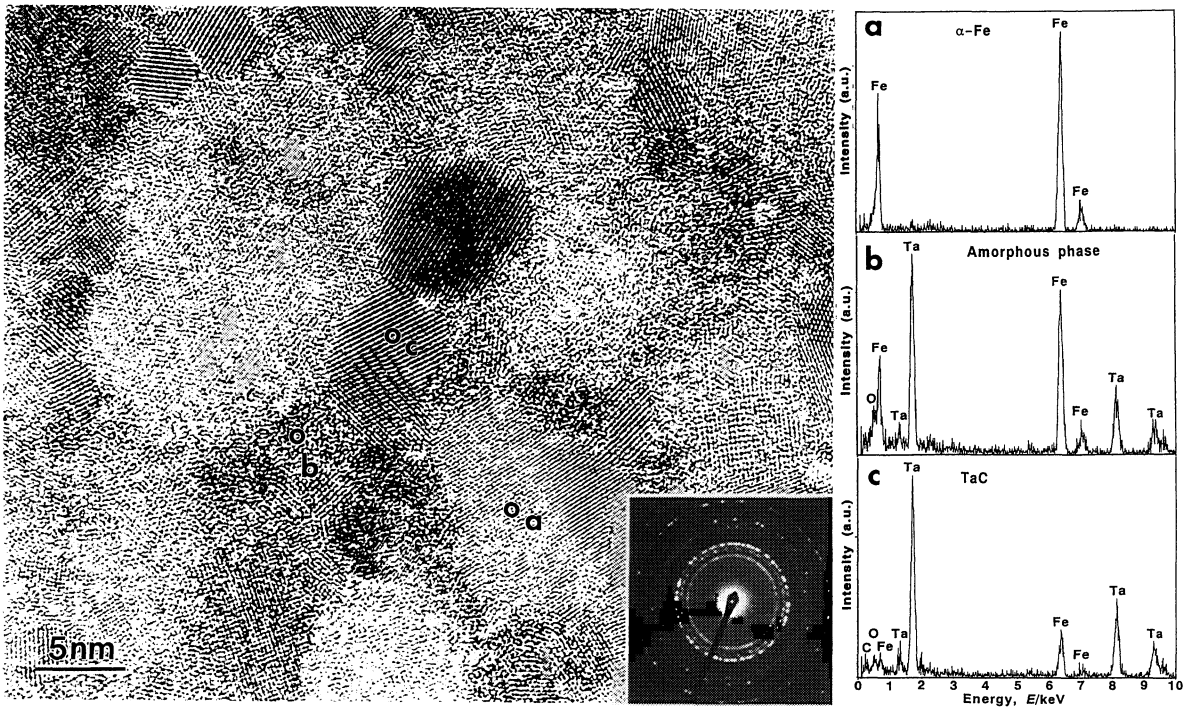

Fig. 11 High-resolution TEM image and nanobeam EDX spectra of the $Fe_{75.4}Ta_{13.1}C_{11.5}$ alloy film annealed at 823 K for 1.2 ks. The EDX spectra a, b, and c were taken from the points indicated with the circles in the photograph.

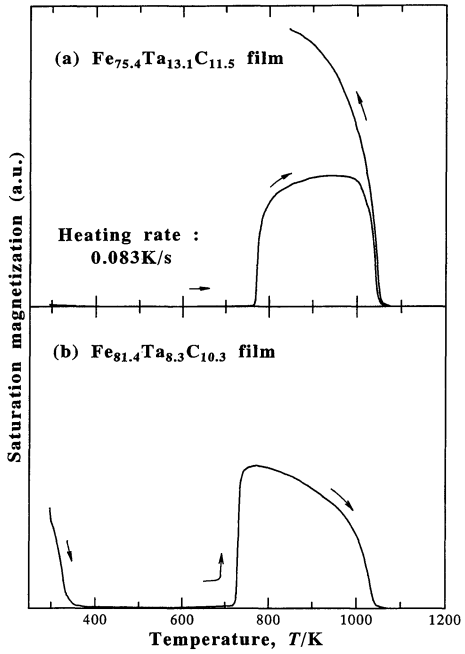

Fig. 12 Temperature dependence of saturation magnetization of as-deposited $Fe_{75.4}Ta_{13.1}C_{11.5}$ (a) and $Fe_{81.4}Ta_{8.3}C_{10.3}$ alloy film (b).

optimum film (b) by about 40 K. After the steep increase, the *Is* of the optimum film (Fig. 12(b)) immediately turns into decrease, suggesting that the transformation is almost completed. On the other hand, the *Is* of the Ta-rich film continues to gradually increase even after steep increase of *Is*. This would be an indication of gradual transformation of the residual amorphous phase.

As previously reported[12], the high-resolution TEM observations of the optimum film suggested the absence of "a detectable amount of" the amorphous phase. Though the high-resolution TEM observation is an effective technique to detect the intergranular phase, the inclination of the boundary layer to the plane of the film often gives an ambiguous result. To obtain more exact information, a nanobeam EDX analysis at an Fe–Fe grain boundary region comparing with that inside the α-Fe grain was performed. If an amorphous phase is present, the intensity of characteristic X-rays of Ta even from the slightly inclined grain boundary region will be higher than that from the center of the grain. Figure 13 shows the high-resolution TEM image and the EDX spectra for the optimum film annealed at 823 K for 1.2 ks. Analyzed points are indicated with the circles in the photograph. The EDX spectrum from the grain boundary region (b) is almost identical to that from the center of the α-Fe grain. Though not shown in the figure, similar analyses performed at three different fields gave the same result. The high intensity of Ta is observed only in the spectrum from the TaC crystals (c) with a wide lattice fringe. As shown in Fig. 14, a clearer TEM image of an Fe–Fe grain boundary can be seen after annealing at a higher temperature (973 K) because the grains are grown larger. This film still exhibits high permeability (1300 at 1 MHz) and low coercivity (65 A/m) in this state, though it is not the

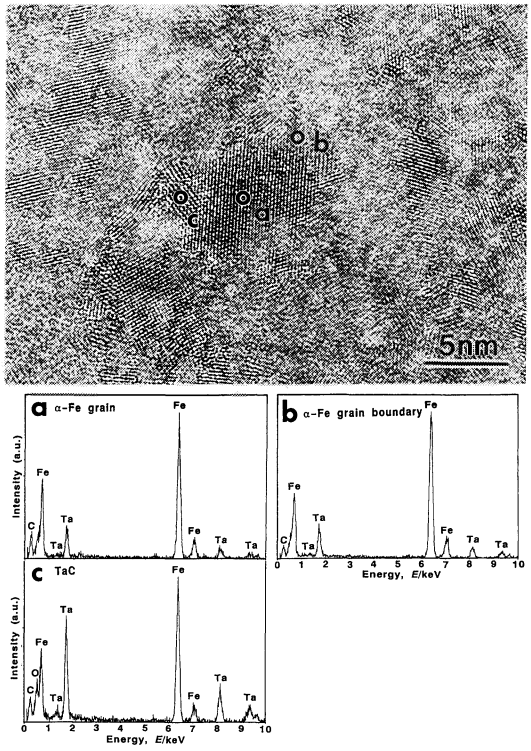

Fig. 13 High-resolution TEM image and nanobeam EDX spectra of the $Fe_{81.4}Ta_{8.3}C_{10.3}$ alloy film annealed at 823 K for 1.2 ks. The EDX spectra a, b, and c were taken from the points indicated with the circles in the photograph.

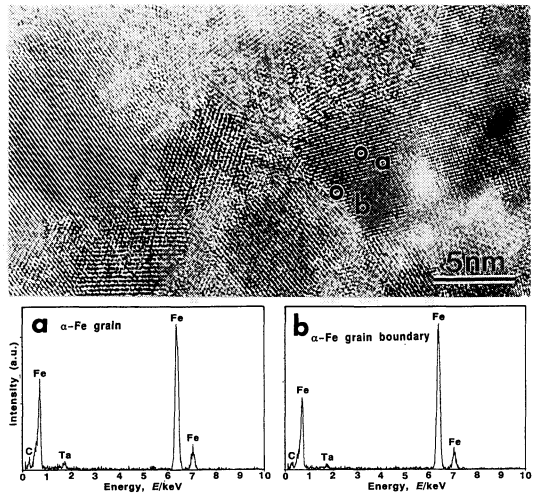

Fig. 14 High-resolution TEM image and nanobeam EDX spectra of the $Fe_{81.4}Ta_{8.3}C_{10.3}$ alloy film annealed at 973 K for 1.2 ks. The EDX spectra a and *b* were taken from the points indicated with the circles in the photograph.

best. The nanobeam EDX spectrum taken from the grain boundary region (b) is again identical to that taken from inside of the grain (a).

It is thus concluded that the important factor for supressing the grain growth of the α-Fe phase in the optimum state for magnetic softness is the presence of TaC nanocrystals at the grain boundaries, rather than the

presence of the residual amorphous phase. The evidence for the role of TaC as a pinning center of grain boundary is obtained by an analysis of the relationship between the grain sizes of α-Fe and TaC[20]. This relationship follows the Zener's relation[21] that characterizes the grain-boundary-pinned growth.

(2) Formation of third phase by high-temperature annealing

The α-Fe and TaC phases in the Fe-Ta-C film annealed around the optimum condition (approx. 750-900 K) are still in metastable states which are a supersaturated solid solution and a non-stoichiometric carbide, respectively[13]. Since these metastable phases have a wide solubility range, another compound such as Fe_3C or Fe_2Ta does not form even in the film with an unequal concentration of Ta to C. However, the third phase will form on annealing at higher temperatures. It is also of interest to examine the effect of the formation of third phase on soft magnetic properties.

The $Fe_{81.4}Ta_{8.3}C_{10.3}$ alloy film, which has been discussed as an example of the optimum composition, also has the unequal concentration of Ta to C. Even after annealing at 973 K, no crystalline phase other than α-Fe or TaC can be seen in the electron diffraction pattern of this film. As already pointed out in the previous paper[12], however, it seems that grain boundaries of this alloy film are not yet in an equilibrium state because they do not look straight in the high-resolution TEM image. Considering slightly C-rich composition of the film, an enrichment of excess C at the grain boundary is plausible. To identify the phase that cannot be detected by the diffractomery, the Mössbauer measurement was carried out. Figure 15(a) and (b) show the Mössbauer spectra of the $Fe_{81.4}Ta_{8.3}C_{10.3}$ alloy films annealed at 823 K and 973 K, respectively. As can be seen in Fig. 15(b), a ferromagnetic sextet appearing in the spectrum of the film annealed at 973 K is divided into Fe and Fe_3C components, while only the Fe component is seen after annealing at 823 K (a). This implies that some Fe atoms, probably around the grain boundary region, are in the same environment as those in a Fe_3C crystal lattice, though they are not yet in a well-defined crystal. A precipitation of Fe_3C generally causes the deterioration of soft magnetic properties, because Fe_3C has an order of magnitude higher magnetocrystalline anisotropy energy than that of Fe[22]. However, the present film maintains good soft magnetic properties as shown in Fig. 16, because the Fe_3C phase in the present film is not in the crystalline form and the effective local anisotropy energy will be sufficiently smaller than that of bulk Fe_3C. By higher-temperature annealing, Fe_3C will form as a crystal.

Figure 16 shows the annealing temperature dependence of coercivity *Hc* of Fe-Ta-C alloy films of various compositions. (The retention time at each annealing temperature is 1.2 ks.) The increase in *Hc* with increasing annealing temperature is most sluggish in the $Fe_{81.4}Ta_{8.3}C_{10.3}$ alloy film which is nearly the optimum composition. The deviation of the Ta to C ratio from this optimum composition leads to the deterioration of the thermal stability of *Hc*. This is attributed to the formation of third crystalline phase, *i.e.* Fe_3C or Fe-Ta compounds.

As an example of the films with more excess C, Fig. 17 shows the TEM imges and electron diffraction pattern of the $Fe_{77.1}Ta_{9.1}C_{13.8}$ alloy film annealed at 1023 K for 1.2 ks. Though a great part of the film consists of nanograins, abnormally grown grains can be seen. A Fe_3C phase together with α-Fe and TaC was identified by the electron diffraction pattern. The growth of such an abnormal grain is probably associated with the formation of Fe_3C because a part of the abnormal grain is illuminated in the dark-field image (b) taken from the reflection of Fe_3C, though a great part of the abnormal grain consists of α-Fe as seen in the dark-field image (a)

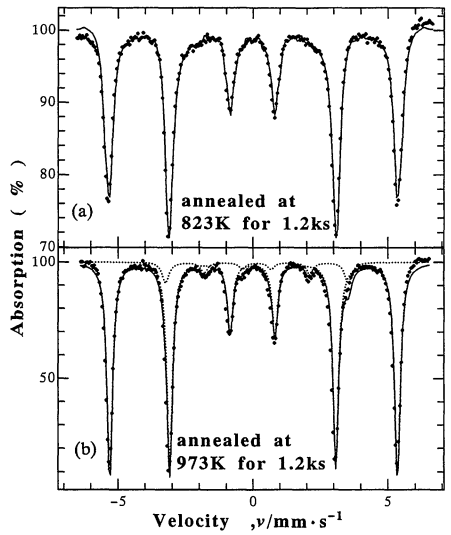

Fig. 15 Mössbauer spectra at room temperature for the $Fe_{81.4}Ta_{8.3}C_{10.3}$ alloy films annealed at 823 K (a) and 973 K (b) for 1.2 ks.

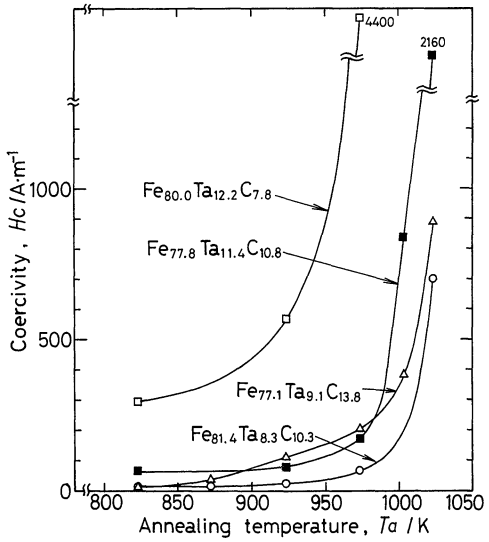

Fig. 16 Annealing temperature dependence of coercivity *Hc* for Fe-Ta-C alloy films with various compositions. (The retention time at each annealing temperature is 1.2 ks.)

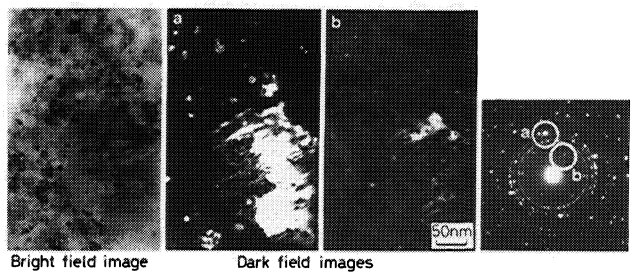

Fig. 17 TEM images and electron diffraction pattern of the $Fe_{77.1}Ta_{9.1}C_{13.8}$ alloy film annealed at 1023 K for 1.2 ks. The dark-field images a and b were taken with an objective aperture indicated with the circles in the diffraction pattern.

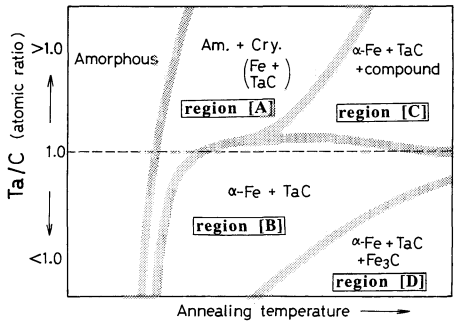

Fig. 19 Schematic chart for the evolution of various phases depending on the ratio of Ta to C in the Fe-Ta-C films. The region [B] is the optimum state for soft magnetic properties.

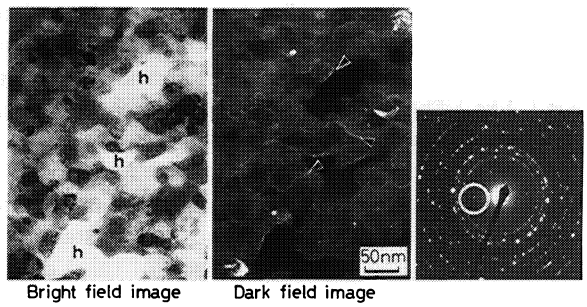

Fig. 18 TEM images and electron diffraction pattern of the $Fe_{75.4}Ta_{13.1}C_{11.5}$ alloy film annealed at 1023 K for 1.2 ks. The dark-field image was taken with an objective aperture indicated with the circle in the diffraction pattern. (The parts indicated with "h" in the bright-field image are the holes in the TEM specimen.)

taken from the reflection of α-Fe. Such structural inhomogeniety and a large magnetocrystalline anisotropy of Fe_3C are the cause of increasing *Hc* for C-excess films.

For the films with excess Ta, on the other hand, the residual amorphous phase will gradually crystallize by higher-temperature annealing as described above. However, soft magnetic properties are not improved at all by the crystallization of the residual phase as shown in Fig. 16. As an example, TEM images and electron diffraction pattern of $Fe_{75.4}Ta_{13.1}C_{11.5}$ film annealed at a sufficiently high temperature (1023 K) are shown in Fig. 18. The film of this composition originally contained a residual amorphous phase after annealing at 823 K, as already described in the previous section. However, there is an unknown phase which is presumed to be a Ta-rich metastable compound in this film annealed at 1023 K. In the dark-field image taken from the reflection of this phase, the grain boundary regions are dimly illuminated as indicated with arrowheads. This phase is probably formed by the decomposition of the residual amorphous phase. If such compounds surrounding Fe grains have poor magnetization, a recovery of soft magnetic properties will hardly be expected.

IV. General Discussion

As a summary, Fig. 19 shows a schematic chart for the evolution of various phases depending on the ratio of Ta to C in the Fe-Ta-C film, though the phase boundaries drawn are not exact. As described in Section III-1, the reaction at an early stage of transformation ("Amorphous"→"region [A]") is the primary crystallization of α-Fe, which is similar to that of the Fe-Cu-Nb-Si-B and the Fe-M-B alloys. Within the region [A], the TaC crystal gradually forms with increasing annealing temperature, at the right part of the region [A], though not explicitly shown in Fig. 19. Except the coexisting state of TaC crystals, the structure in the region [A] is quite similar to the optimum state of the Fe-Cu-Nb-Si-B and the Fe-M-B alloys. The growth of α-Fe grain is mainly retarded by residual amorphous phase rather than by TaC at this state. However, soft magnetic properties of the present alloy in the region [A] is not in the optimum state, because the residual amorphous phase has only a low magnetization resulting in an insufficient intergranular coupling. The optimum state for magnetic softness is in the region [B] where the residual amorphous phase is absent. While the region [A] for the Fe-Cu-Nb-Si-B and the Fe-M-B alloys covers a wide annealing temperature range, the region [A] for the optimum composition in the present alloys has only a narrow range. Such a difference is most likely caused by a stronger reactivity between Ta and C toward TaC, that is a lower free energy in TaC, than that between M(=Nb, Zr, Hf, etc.) and B. In the Fe-Cu-Nb-Si-B and the Fe-M-B alloys, no M-boride crystals appear in the course of annealing even at high temperatures, but Fe-boride appears instead. Since the TaC grains precipitate as small particles at the grain boundaries of α-Fe, they enable the direct contact between indivisual α-Fe grains and further stabilize the nanograins of α-Fe, resulting in an optimum soft magnetic properties.

The expanded area of the region [A] at the Ta-rich side is due to the stabilization of the amorphous phase by residual Ta atoms remaining after the reaction between Ta and C. However, such a residual amorphous phase deteriorates the magnetic softness as described above. The transformation into the region [C] from [A], which is the decomposition of the residual amorphous phase into unknown compound (and α-Fe), is so gradual that the phase boundary drawn in Fig. 19 is uncertain.

The reaction into the region [D] from [B] will be the decomposition of α-Fe containing supersaturated C into Fe_3C and α-Fe. Near the optimum film composition, the rejected C atoms from α-Fe is probably absorbed into TaC which was originally a non-stoichiometric C-poor compound to approach the stoichiometric TaC, as previously reported[13]. However, a high C concentration exceeding the stoichiometric composition causes such decomposition. As a result the best thermal stability of soft magnetic properties is realized near the equal concentration of Ta and C.

V. Conclusion

The nanocrystallization process of amorphous Fe-Ta-C alloy films as well as the structural evolution by further annealing and its relation to soft magnetic properties are studied. The resuls obtained are as follows:

(1) Similarly to the nanocrystallization of other amorphous alloys, the transformation at the first stage for these alloys is the primary crystallization of α-Fe. The formation of TaC crystals follows this reaction, though some bonding between Ta and C seems to be already present.

(2) In the early stage, the growth of α-Fe grain is considered to be controlled by diffusion of Ta out of α-Fe to the amorphous matrix. However, the residual amorphous phase is almost absent after the optimum annealing of the film with the optimun composition. In such a state, TaC particles stabilize the nanograins instead.

(3) The analysis of kinetics suggests that the nucleation mechanism of the nanocrystallization in Fe-Ta-C alloys is different from that in the other alloys. Further, the nucleation mechanism and growth morphology are independent of temperature unlike the Fe-M-B alloys. This results in the easiness in obtaining good soft magnetic properties without imposing any strict condition on the heat treatment.

(4) At the optimum composition, that is, near the equal concentration of Ta and C, further transformation does not occur. Soft magnetic properties are maintained even after high-temperature annealing and are only gradually deteriorated by gradual grain growth retarded by grain boundary pinning by TaC. This is also an advantage over the other nanocrystalline alloys whose softness abruptly decreases when the secondary crystallization takes place.

(5) The decrease in thermal stability of magnetic softness for the films outside the optimum composition is associated with the formation of a third phase.

Acknowledgments

The authors are grateful to Dr. K. Hono of IMR, Tohoku Univ. (presently at Nat. Res. Inst. for Metals) for helpful discussions. We also wish to thank Mr. H. Adachi and Mr. D. Kawase, formerly graduate students of Tohoku Univ., for their help in the Mössbauer and the DSC measurements, respectively. Thanks are also due to Mr. K. Ohminato of Alps Electric Co., Ltd. for HRTEM technical assistance.

REFERENCES

(1) Y. Yoshizawa, S. Oguma and K. Yamauchi: J. Appl. Phys., **64** (1988), 6044.
(2) K. Suzuki, N. Kataoka, A. Inoue and T. Masumoto: Mater. Trans., JIM, **31** (1990), 743.
(3) K. Suzuki, A. Makino, A. Inoue and T. Masumoto: J. Appl. Phys., **74** (1993), 3316.
(4) A. Inoue, T. Ochiai, Y. Horio and T. Masumoto: Mater. Sci. Eng., **A179/A180** (1994), 649.
(5) Y. H. Kim, K. Hiraga, A. Inoue, T. Masumoto and H. H. Jo: Mater. Trans., JIM, **35** (1994), 293.
(6) K. Hono, K. Hiraga, Q. Wang, A. Inoue and T. Sakurai: Acta Metall. Mater., **40** (1992), 2137.
(7) U. Köster, U. Schünemann, M. Blank-Bewersdorff, S. Brauer, M. Sutton and G. B. Stephenson: Mater. Sci. Eng., **A133** (1991), 611.
(8) K. Suzuki, A. Makino, A. P. Tsai, A. Inoue and T. Masumoto: Mater. Sci. Eng., **A179/A180** (1994), 501.
(9) K. Suzuki, A. Makino, A. Inoue and T. Masumoto: Sci. Rep. RITU, **A39** (1994), 133.
(10) N. Hasegawa and M. Saito: J. Magn. Soc. Jpn., **14** (1990), 313; IEEE Translation J. Magn. Jpn., **6** (1991), 91.
(11) K. Hono, N. Hasegawa, S. S. Babu, H. Fujimori and T. Sakurai: Appl. Surf. Sci., **67** (1993), 391.
(12) N. Hasegawa, N. Kataoka, K. Hiraga and H. Fujimori: Mater. Trans., JIM, **33** (1992), 632.
(13) N. Hasegawa, M. Saito, N. Kataoka and H. Fujimori: J. Mater. Eng. & Performance, **2** (1993), 181.
(14) W. A. Johnson and R. F. Mehl: Trans. Am. Inst. Min. Eng., **135** (1939), 416.
(15) M. Avrami: J. Chem. Phys., **7** (1939), 103; **8** (1940), 212; **9** (1941), 177.
(16) H. K. Lachowicz, M. Kuzminski, T. Kulik and A. Hernando: NanoStructured Materials, **4** (1994), 865.
(17) J . W. Christian: *The Theory of Transformations in Metals and Alloys*, Pergamon Press, Oxford, (1965), p. 542.
(18) N. Kataoka, A. Inoue, T. Masumoto, Y. Yoshizawa and K. Yamauchi: Jpn. J. Appl. Phys., **28** (1989), L1820.
(19) G. Herzer: IEEE Trans. Magn., **25** (1989), 3327.
(20) N. Hasegawa, N. Kataoka and H. Fujimori: to be published.
(21) C. Zener, cited by C. S. Smith: Trans. AIME, **175** (1948), 15.
(22) P. Blum and R. Pauthenet: CR Acad. Sci., **237** (1953), 1501.